J. Fluid Mech. (1993), *vol.* 247, *pp.* 111–136

Boundary interactions for two-dimensional granular flows. Part 1. Flat boundaries, asymmetric stresses and couple stresses

By CHARLES S. CAMPBELL

Department of Mechanical Engineering, University of Southern California, Los Angeles, CA 90089-1453, USA

(Received 26 July 1990 and in revised form 6 August 1992)

The behaviour of a granular flow at a boundary cannot be specified independently of what is happening in the rest of the flow field. This paper describes a study of two fictitious, but instructive, flat boundary types using a computer simulation of a two-dimensional granular flow with the goal of trying to understand the possible effects of the boundary on the flow. The two boundary conditions, Type A and Type B, differ largely in the way that they apply torques to the flow particles. During a particle–wall collision, the Type A boundary applies the force at the particle surface, thus applying the largest mechanistically possible torque to the particle, while the Type B boundary applies the force directly to the particle centre, resulting in the application of zero torque. Though a small change on continuum scales (i.e. the point at which the force is applied has only been moved by a particle radius) it makes a huge difference to the macroscopic behaviour of the system. Generally, it was found that, near boundaries, large variations in continuum properties occur over distances of a particle diameter, a non-continuum scale, throwing into doubt whether boundaries may be accurately modelled via continuum mechanics. Finally, the large torques applied to the particles by the Type A boundary induce asymmetries in the stress tensor, which, in these steady flows, are balanced by gradients in a couple stress tensor. Thus, near boundaries, a frictional granular material must be modelled as a polar fluid.

1. Introduction

Conventional fluid mechanics has the luxury of a no-slip condition, which requires that the velocity of the fluid immediately adjacent to a solid boundary assumes the velocity of the boundary. This allows the mechanical properties of the material at the boundary to be specified independently of whatever is happening in the rest of the flow field. Granular materials are not so blessed and the flow behaviour at a solid or free surface is an integral part of the solution for the entire flow field. For example, there will generally be velocity slip at the boundary which is determined by the manner in which the flow interacts with the boundary and thus acts to match the physical nature of the boundary with the flow far from the boundary.

A strong effect of the boundary characteristics has also been noted experimentally. Savage & Sayed (1984) and Hanes & Inman (1985) both performed nearly identical shear cell tests on nearly identical materials. The only major difference between the two studies was the way in which their bounding walls were roughened. (In this type of device, walls are roughened in order to make a good mechanical contact between

the test material and the driving surfaces.) Yet Hanes & Inman measured stresses that were up to three times larger than Savage & Sayed for otherwise equivalent conditions. Similarly, Craig, Buckholtz & Domoto's (1987) study of the effects of shear cell boundary conditions indicates that the condition of the drive surfaces often has a larger impact on the measurement than the material tested. Differences in the boundary may also explain discrepancies in some chute flow experiments and simulations. For example, the boundary characteristics could explain the presence of the inflexion point observed in the chute flow velocity profiles measured by Savage (1979) and Ishida & Shirai (1979) that were missing from those measured by Bailard (1978), Campbell & Brennen (1985*b*), Drake & Shreve (1986) and Augenstein & Hogg (1978). Also, the corresponding solid fraction profile observed by Campbell & Brennen (1985*b*), Bailard (1978) and Ridgway & Rupp (1970) show a low-density zone near the chute bottom that is nearly absent from the data of Ahn, Brennen & Sabersky (1991). The different results may be attributed not only to the character of the boundary but also to the fact that these studies were performed on different materials that may interact with similar boundaries in very different ways. Also, Zhang & Campbell (1992), have studied the special type of boundary that forms between flowing and stagnant regions of a granular flow.

Several theoretical studies have incorporated boundary conditions into the solution of simple flow fields. The first of these, Hui *et al.* (1984), modelled the wall interaction as an equivalent roughness coefficient, but neglected the shear work performed by the boundary due to the velocity slip at the surface. Jenkins & Richman (1986) developed a set of boundary conditions for two-dimensional smooth circular disc flows in the neighbourhood of a boundary composed of semicircular bumps glued to a flat wall. However, a complication became apparent in examining the corresponding solutions to Couette flow problems. The results showed that, for a given separation distance between the driving surfaces, a steady flow was possible for one and only one average value of the solid fraction. In contradiction, shear cell experiments and computer simulations of these flows indicate that steady flows are possible for any average concentration. This work was later extended by Richman & Chou (1988) and by Richman (1988). These latter two works suggested a heuristic solution to the uniqueness problem by not strictly applying the continuity of normal stress at the boundary. But the resolution of the uniqueness problem was found by Hanes, Jenkins & Richman (1988). They noted that, as the presence of a wall causes a local distortion in the arrangement of particles in its immediate vicinity, the concentration of the flow in the immediate neighbourhood of the boundary could be a free parameter to be determined as a matter of course in the application of the boundary conditions. Allowing the density at the wall to vary introduced enough freedom in the solution to allow steady flows at any average concentration. (It turns out that this solution to the problem is essentially equivalent to the heuristic arguments used by Richman & Chou 1988 and Richman 1988.)

An extremely strong effect was also noted in the computer simulation studies of Couette flows performed by Campbell & Brennen (1985*a*). In this early work, they characterized the wall–particle interaction by assuming that, on departure after a collision with the wall, there was no relative velocity between the wall and the contact point on the particle, i.e. there was no slip between the particle surface and the wall. This, they referred to as a 'Type A' boundary. Because the collision impulse is applied at the edge of the particle rather than the centre, the particle experiences a torque which induces large rotation of the particle. One drawback of this scheme is that the particle more or less rolls over the wall, allowing a great deal of slip

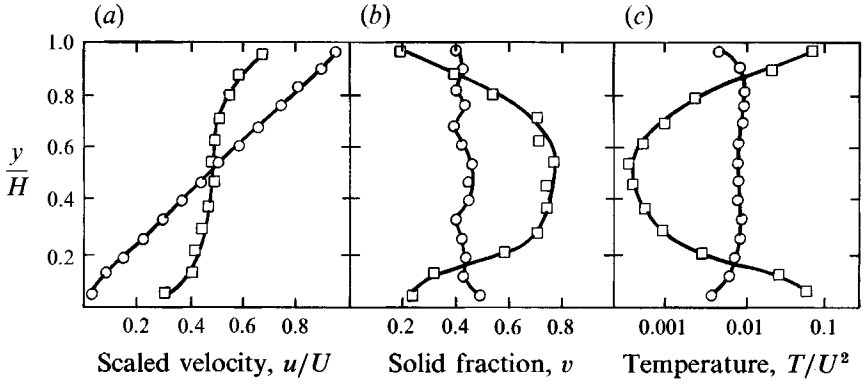

FIGURE 1. Type A (□) and B (○) boundary conditions comparisons. Data taken from Campbell & Brennen (1985*a*). (For the Type A condition, $\bar{\nu} = 0.53$, for the Type B condition, $\bar{\nu} = 0.45$.)

between the velocity of the particle centre and that of the wall. Under such conditions the bulk shear rate becomes somewhat independent of the wall velocities. With the sole intent of gaining control of the imposed shear rate, Campbell & Brennen introduced an alternative boundary condition which assumed that, on departure after a collision with a wall, the particle centre assumes the same velocity as the wall, i.e. there is no slip between the particle centre and the wall with no change in the rotation rate. This they called the 'Type B' boundary condition. One essential difference with the Type A condition is that the Type B condition does not provide a torque to the particle and does not induce a large rotation at the wall.

This may seem to be a minor change – the application point of the force has been moved only a particle radius, which should be insignificant on continuum lengthscales – but it has a dramatic effect on the flow field. Figure 1 shows some of the two-dimensional Couette flow data take from Campbell & Brennen (1985*a*). The simulation from which this is derived is nearly identical to that used in the current study (which is shown in figure 3 and will be discussed later). Figure 1 (*a*) shows the profile of the average velocity, $\langle u \rangle$, normalized by the top wall velocity, U. Figure 1 (*b*) shows the corresponding distribution of the solid fraction, ν, which is a dimensionless density that laterally means the fraction of a unit area covered by solid material. Figure 1 (*c*) shows the distribution of the 'granular temperature', T, which is twice the kinetic energy per unit mass associated with the random velocity of the particles and has been shown to fill a similar role in rapid granular flows as the thermodynamic temperature does in gases and liquids. (For more information on how these quantities are found, the reader is referred to Campbell & Brennen 1985*a*.) Please note that the granular temperature as plotted throughout this paper includes the fluctuating rotational velocity. Also, note that in this plot as in Campbell & Brennen (1985*a*) the granular temperature is scaled by dividing by the square of the top wall velocity, U. (A different scaling for the granular temperature will be used for the data presented later in this paper.) The vertical axis for all three plots is the vertical coordinate, y, divided by the shear gap thickness, H. The two sets of data were taken for as close to the same wall velocity, shear gap thickness, and overall solids concentration as appears in the Campbell & Brennen data; the most significant difference between them is the wall boundary condition.

The results for the Type A condition show the expected slip velocity at the wall. In addition, there are relatively large velocity gradients near the wall, corresponding

to which are regions of reduced density and large granular temperature. (This clearly illustrates the similarities between the granular and thermodynamic temperatures. Simply put, as there is no vertical acceleration of the system, the normal stress must be constant across the shear gap; the large granular temperature allows the applied stress to be borne by a reduced particle concentration in much the same way as an elevated thermodynamic temperature allows a gas at a reduced density to resist a given pressure.) The source of the large granular temperature near the wall is, at least in part, a function of the low density and large velocity gradients. First of all, the large velocity gradients imply larger impact velocities, and, as the random velocity generated in a collision is proportional to the impact velocity, one also expects larger granular temperatures. Now, while granular temperature is generated in collisions, it is also being dissipated by the collisional inelasticity. A reduced particle concentration implies a smaller collision rate with consequently smaller temperature dissipation; hence, one expects larger granular temperatures in regions of reduced density. (This temperature generation/dissipation process is described in detail in the review article by Campbell 1990.) Furthermore, to complete the circle, as the shear stress must be constant across the channel, larger velocity gradients are required to transfer the shear stress in regions of reduced density.

On the other hand, the Type B profiles are vastly different. First of all, as might be expected from the construction of the boundary condition, there is no slip velocity at the walls. However, unlike the Type A condition, these flows show a roughly uniform velocity gradient, density and temperature across the channel. Note also that, as the mean velocity gradient is larger than for the Type A boundary, the average magnitude of the granular temperature is correspondingly increased. The same arguments used above can be applied here: because the velocity gradient and solid fraction are uniform, the granular temperature is uniform which in turn permits a uniform velocity gradient. (In their inclined chute flow simulations, Campbell & Brennen (1985*b*) showed similar behaviour for the same two boundary conditions.)

Note that the Type A boundary acts as a source of granular temperature. The largest temperatures occur near the wall and the large temperature gradient leading away from the walls indicate a conduction of temperature towards the centre of the channel. The Type B boundary shows a slight temperature deficit at the wall. On one level, this indicates that the boundary is acting as a temperature sink. However, the effect is confined to the immediate vicinity of the wall and, as far as the bulk of the flow is concerned, the granular temperature is uniform. Hence, from a continuum viewpoint, the Type B boundary appears to be neutral and neither a source nor a sink of granular temperature – at least under these flow conditions.

While this explains the interconnection between the velocity, density and temperature profiles, it does not account for why one behaviour is associated with the Type A boundary condition and the other with the Type B. The observations presented in the rest of this paper indicate that the controlling factor is the way that the boundary transmits torque to the particles. The Type A boundary imparts a large rational speed to the particles which is roughly equal to the slip velocity divided by the particle radius. As this rotation is a coherent and not a random velocity, it is, itself, not a contribution to the granular temperature. However, on subsequent collisions, the frictional coupling between the particle surfaces will transfer this coherent rotational velocity into both rotational and translational velocities; the resulting particle velocities depend on the geometry of the particular collision, and, thus, in a macroscopic sense, will be randomly distributed and appear as granular temperature. Thus, the large rotational imposed at the wall provides a local source

of granular temperature; the high granular temperature forces a lower density and larger velocity gradients, all of which feed back to further elevate the granular temperature. The Type B boundary applies no rotation and thus does not act as a temperature source. Without this large temperature source, conduction-like processes even out the internal granular temperature and allow uniform velocity gradients and solid fraction distributions.

This paper studies this problem in much greater detail, paying particular attention to the ways that torques are applied to the particles. While the Type A and Type B boundaries are somewhat fictitious, they are ideal for this purpose as they represent extremes in how they apply torque to the particles; by not allowing slip between the particle surface and the wall the Type A boundary applies the maximum, mechanistically possible, torque to the particles while, by its definition, the Type B boundary applies zero torque. In this way, I hope to highlight important features of the flow field/boundary interaction. A companion paper, Campbell (1993) will study more realistic boundary conditions created by gluing solid particles to walls. A preliminary (and not entirely correct) report of this work appears in Campbell (1988).

2. Computer simulation

This study is performed in a computer simulation that is nearly identical to that used by Campbell & Brennen (1985*a*) and so will only be briefly described here. The situation studied is a Couette flow of two-dimensional discs, each with mass m and radius R, trapped in a control volume which is shown schematically in figure 2. The control volume is bounded on the top and bottom by solid walls which are separated in the y-direction by a distance H. To induce a shear flow the top wall is set in motion in the x-direction with a velocity U relative to the bottom. As in Campbell & Brennen's (1985*a*) simulation, the spacing of the solid walls is not fixed. Instead, a normal force is applied to the boundary and the spacing of the boundary adjusts itself to balance the applied force. One enhancement incorporated into the current simulation is a control scheme that periodically checks the wall spacing and varies the applied normal force to keep the wall spacing nearly fixed. The scheme is based on Bagnold's (1954) finding that the stresses vary with the square of the shear rate so that, with the wall velocity held constant, the stress varies as the inverse square of the wall separation; with that concept in mind, the applied normal stress is periodically varied as the square of the ratio of the current and desired wall separations. These simulation used a wall spacing of forty particle radii (unless otherwise specified). In the direction of flow, the control volume is bounded by periodic boundaries. This is realized in the simulation by dictating that when a particle exits the downstream periodic boundary, it re-enters the upstream boundary with exactly the same y-coordinate and velocity with which it left, thus simulating a case in which the control volume is periodically repeated, infinitely many times, up- and downstream. Once started, the simulation is allowed to progress until it reaches a steady state. From that point on, the properties of the system are averaged to obtain whatever information is required.

The particles interact by colliding with one another. Each collision is assumed to occur instantaneously once the particle surfaces come into contact (this is essentially the hard-sphere approximation often used in the kinetic theory of gases) and the collision result is computed from a standard centre-of-mass collision solution. Because the particles rotate as well as translate, two conditions are required to close the system of equations: one for the relative particle velocities normal to and one for

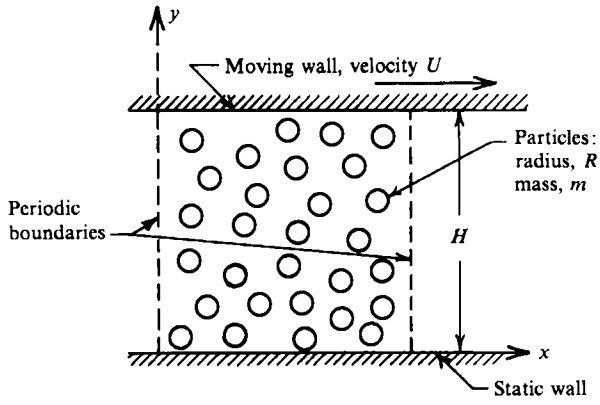

FIGURE 2. Schematic of the simulated system.

the velocities tangential to the particle surfaces at contact. The normal velocity condition assumes that the particles are 'nearly elastic' in the sense that energy is dissipated as a result of the collision, but the particles retain their circular shape. This is realized in the simulation through a coefficient of restitution, e ($e = 0.8$ is used throughout this study), which is the ratio of the approach to recoil velocities, and is specified as an input parameter to the program. For the tangential condition, the particle surfaces are assumed to interact frictionally. The impulse, $\boldsymbol{J}$, exerted by the collision is then

$$\boldsymbol{J} = \boldsymbol{J}_{\mathrm{N}} + \boldsymbol{J}_{\mathrm{T}}. \tag{2.1}$$

Here $\boldsymbol{J}_{\mathrm{N}}$ represents the collisional impulse normal to the point of contact:

$$\boldsymbol{J}_{\mathrm{N}} = \tfrac{1}{2}m(1+\epsilon)\,(\boldsymbol{q}\cdot\boldsymbol{k})\,\boldsymbol{k}, \tag{2.2}$$

where m is the mass of the particle, ϵ is the coefficient of restitution, $\boldsymbol{q} = \boldsymbol{u}_1 - \boldsymbol{u}_2$ is the relative velocity of the particles just before collision, and $\boldsymbol{k} = (\boldsymbol{x}_2 - \boldsymbol{x}_1)/\|\boldsymbol{x}_2 - \boldsymbol{x}_1\|$ is the unit vector pointing along the line connecting the particle centres at the instant of collision. (Here, $\boldsymbol{x}_1$ and $\boldsymbol{x}_2$ are vectors pointing from the origin to the centres of particles 1 and 2 respectively and $\boldsymbol{u}_1$ and $\boldsymbol{u}_2$ are the translational velocities of the particles immediately prior to collision.) $\boldsymbol{J}_{\mathrm{T}}$ is the impulse tangential to the point of contact. To incorporate a surface friction coefficient, the value of $\boldsymbol{J}_{\mathrm{T}}$ is found by a two-step process. First, the impulse is computed assuming that there would be no tangential slip between the particle surfaces. This test case will be called $\boldsymbol{J}'_{\mathrm{T}}$ and is defined

$$\boldsymbol{J}'_{\mathrm{T}} = \frac{m\beta}{2(1+\beta)}(\boldsymbol{q} - (\boldsymbol{q}\cdot\boldsymbol{k})\,\boldsymbol{k} + R(\boldsymbol{\omega}_1 + \boldsymbol{\omega}_2)\times\boldsymbol{k}), \tag{2.3}$$

where $\boldsymbol{\omega}_1$ and $\boldsymbol{\omega}_2$ are the particle angular rotation rates, β is the ratio of the square of the particle radius of gyration to the square of the particle radius. The value of $\|\boldsymbol{J}'_{\mathrm{T}}\|$ is then compared against the value computed for $\|\boldsymbol{J}_{\mathrm{N}}\|$ to see if the ratio exceeds a specified surface friction coefficient μ. If the surface friction is not exceeded, then there will be no slip between the particle surfaces and $\boldsymbol{J}_{\mathrm{T}}$ is set equal to $\boldsymbol{J}'_{\mathrm{T}}$, i.e.

$$\text{If} \qquad \|\boldsymbol{J}'_{\mathrm{T}}\|/\|\boldsymbol{J}_{\mathrm{N}}\| < \mu \quad \text{then} \quad \boldsymbol{J}_{\mathrm{T}} = \boldsymbol{J}'_{\mathrm{T}}. \tag{2.4}$$

However, if μ is exceeded, the tangential impulse is chosen to have a magnitude of $\mu\|\boldsymbol{J}_{\mathrm{N}}\|$, acting in the direction of $\boldsymbol{J}'_{\mathrm{T}}$, i.e.

If $$\|\boldsymbol{J}_{\mathrm{T}}'\|/\|\boldsymbol{J}_{\mathrm{N}}\| > \mu \quad \text{then} \quad \boldsymbol{J}_{\mathrm{T}} = \mu\|\boldsymbol{J}_{\mathrm{N}}\|\,\boldsymbol{J}_{\mathrm{T}}'/\|\boldsymbol{J}_{\mathrm{T}}'\|. \tag{2.5}$$

The value of μ for particle–particle collisions can be specified independently of its value, μ_{w}, for particle–wall collisions. Except where explicitly stated, all of the results in this paper were computed for an infinite surface friction coefficient (i.e. on departure, after a collision, there is no slip between the particle surfaces or, equivalently, (2.3) always holds), just as in Campbell & Brennen (1985*a*).

Properties are averaged by dividing the control volume into imaginary strips, which are slightly larger than a particle diameter wide in the y-direction and span the control volume in the x-direction. At specific intervals, the properties of the particles occupying the strip are sampled and the average over many thousands of sampling periods yields the value attributed to that strip. The contribution from a particle only partially occupying a strip is weighted by the portion of the particle that lies within the strip. The interval between samples is roughly the time it takes each particle in the simulation to undergo one collision. A more detailed discussion of the averaging procedure is given in Campbell (1982). It is debatable whether values, so averaged, may be considered to be the corresponding 'continuum' quantities, especially when (as shall be shown) the sampled quantities vary strongly over the non-continuum lengthscale of a particle diameter (which is approximately an averaging strip width); in other words, is this appropriate averaging of the particle properties to yield what would be considered to be continuum values? This is nearly a philosophical issue, and, as far as this paper is concerned, is irrelevant. It is sufficient to understand that, in this paper, the plotted values are simply averages of the properties of the particles that reside in these imaginary strips and not to try and give them any larger meaning.

3. General features of the flow field

Figures 3, 5 and 6 show comparisons of the Type A and Type B boundary conditions for three different concentrations, $\bar{\nu} = 0.65$, 0.45 and 0.15. The figures are similar in form to figure 1, but, in addition, show the distribution of scaled rotation rate, $-\omega H/U$. (Note that, here, as in the rest of this paper, the granular temperature, T, which has units of (velocity)^2, has been scaled by the apparent velocity gradient, U/H, so that it appears in the dimensionless form TH^2/R^2U^2.) Consider first figure 3, which shows the results of simulations for an average solid fraction, $\bar{\nu} = 0.65$. Notice that the differences between the Type A and B boundary conditions are not as dramatic as one would have expected from the results of Campbell & Brennen (1985*a*) – such as those reproduced in figure 1. Here, with the exception of no slip at the walls, the Type B condition shows many of the near-wall features associated with the Type A condition: larger velocity gradients, smaller densities and elevated temperatures – although to a significantly reduced degree. This indicates that, under these conditions, both boundaries are acting as temperature sources, and as will be argued in the following, this behaviour may be attributed to the way in which the boundaries apply torque to the particles.

Figure 3(*c*) shows the average rotational state of the particles, which is the only information not reported in Campbell & Brennen (1985*a*) and, as suggested above, may hold the key to the entire story. The Type A profiles show a large rotation rate at the boundaries which is to be expected because of the large torque that the boundary applies to the particles. Near the centre of the channel the rotation rate is nearly uniform, but, near the wall, the rotation rate varies dramatically over scales

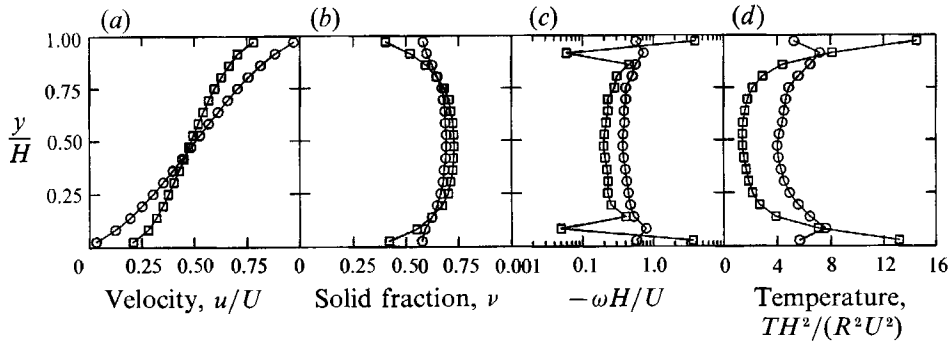

FIGURE 3. Comparison of the Type A (□) and B (○) boundary conditions for an average solid fraction $\bar{\nu} = 0.65$.

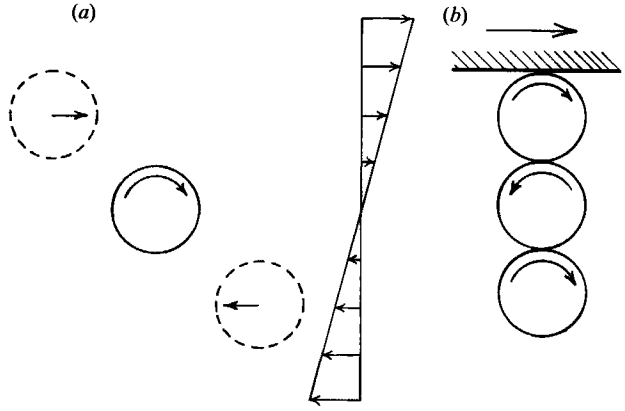

FIGURE 4. The two interacting mechanisms that collectively determine the rotational state of the particles. (*a*) Shear-induced rotation, (*b*) perturbation imposed near the wall.

of the order of a particle diameter (remember that the points are separated by the averaging strip width which is approximately a particle diameter). This behaviour can be explained as a competition between two mechanisms of angular momentum generation that are illustrated in figure 4. First (figure 4*a*), in any shear flow a particle will primarily collide either with faster particles from above and behind or with slower particles in front and below. Both types of collision will induce a clockwise rotation of the particle and Campbell & Gong (1986) have shown that the mean rotation rate will be approximately one half the shear rate – except at extreme values of the particle concentration. (Note that in the centre of the channel, the average rotation rate is, indeed, about half the local shear rate.) On colliding with a wall, however, the particle will pick up a large rotational velocity which is proportional to the slip velocity. Subsequent collisions will induce a counter-rotation in the particles residing in the next layer further out from the wall, resulting in slower rotation. These particles, in turn, induce their own counter-rotation in the next layer out so that those particles exhibit a slightly larger rotation rate. This process is illustrated in figure 4(*b*). The rotational interchange continues until the wall effect (figure 4*b*) finally gives way to the mean shear effect (figure 4*a*). (Note that the mechanism illustrated in figure 4(*b*) will, most likely, have a stronger influence in these two-dimensional disk flows than for three-dimensional spheres, as the disks are all confined to the same plane.)

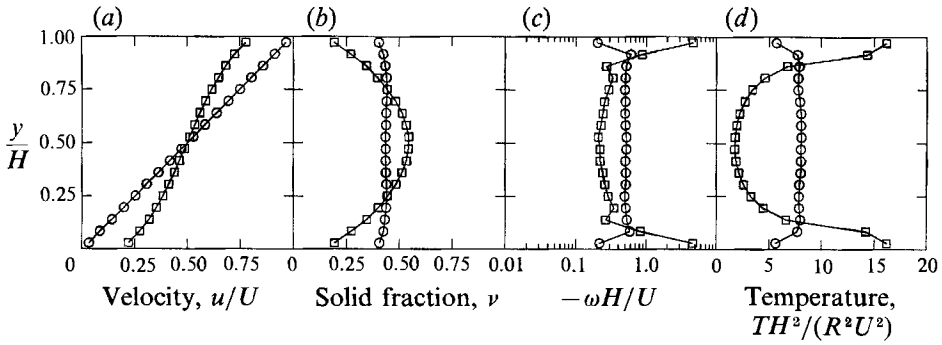

FIGURE 5. Comparison of the Type A (□) and B (○) boundary conditions for an average solid fraction, $\bar{\nu} = 0.45$.

The rotational velocity profile for the Type B boundary condition is much more uniform across the channel, although it still exhibits a similar, though far less pronounced, jagged shape near the walls. Note, however, that the jags are exactly out of phase with the Type A curve. It is a bit strange that there is any effect of the Type B boundary as, unlike the Type A boundary, it exerts no torque to change the rotational state of the particles. But, at the same time, this behaviour may still be understood in terms of the discussion above. As shown in figure 4(*a*), a particle far from the walls will collide with faster particles from above and slower particles from below, both of which will induce clockwise rotation. Any boundary will block collisions on one side of the particles very near by, and, as the Type B boundary itself exerts no torque, those particles experience a smaller net torque than for those further away, resulting in a smaller average rotation rate right next to the wall. Then, following exactly the same logic as above, subsequent collisions will induce a counter torque and, hence, a slightly larger rotational velocity in the particles one layer away from the wall. This, in turn, will induce a slightly lower rotational velocity in the next layer out and so on. Thus, even though the Type B boundary does not transmit any torque, it has much the same effect as it causes a discontinuity in the distribution of angular momentum internal to the material. This will be discussed in more detail in the description of couple stress that is to follow.

Note that this rotational interchange, so important to the generation of granular temperature, occurs over lengthscales of the order of a particle diameter. That continuum properties vary so drastically over non-continuum lengthscales raises the question of whether continuum mechanics can be successfully applied to the boundary problem.

Figure 5 shows the same type of comparison as in figure 3 for a slightly lower average solid fraction, $\bar{\nu} = 0.45$. Note that, in this figure, the characteristics of the Types A and B boundary conditions have returned to the behaviour expected from Campbell & Brennen (1985*a*); i.e. the velocity gradient, density and temperature in the type B simulation are nearly uniform across the shear gap, while the Type A still shows elevated velocity gradients, elevated temperatures, and reduced density in the neighbourhood of the boundary. Also, while the rotational profiles still show the jagged behaviour near the wall, the size of the jags is much smaller than for the higher density results shown in figure 3. This indicates a diminished importance of the mechanism of rotational exchange illustrated in figure 4(*b*). But that should not be surprising: for that mechanism to operate, a particle must collide with another and exchange its rotational state, soon after it has collided with the wall. The lower

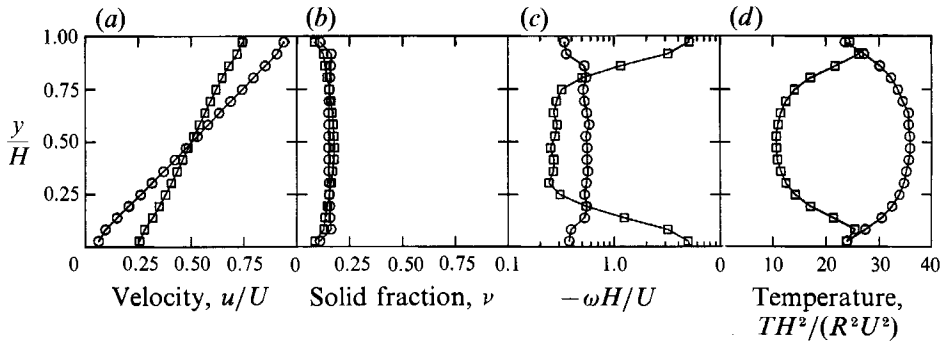

FIGURE 6. Comparison of the Type A (□) and B (○) boundary conditions for an average solid fraction, $\bar{\nu} = 0.15$.

the concentration, the more likely that a particle will move further away from the wall before its next collision, thus diffusing its rotation further away from the wall. In this light, note that the first jag in the rotational velocity profile appears in the second point going outward from the wall in figure 5, while it appears in the point immediately adjacent to the wall in figure 3. Apparently, the particle concentration at the wall of figure 5 is small enough to keep the mechanism of figure 4(*b*) from taking effect until a region of higher concentration is encountered.

This rotational diffusion-like process is much easier to discern in figure 6. Here the average solid fraction is only $\bar{\nu} = 0.15$ and, as the particles travel long distances between collisions, the flow might be considered to be the granular equivalent of a gas. Note that the results of figure 6 look vastly different from those in figures 3 and 5. Both the velocity gradient and solid fraction are nearly uniform across the channel, even for the Type A boundary; in fact, except for the slip velocity, these Type A profiles nearly mirror the Type B. However, the rotational and granular temperature profiles for the Type A and Type B boundaries are very different from each other. This behaviour might be understood as the logical extension of the last paragraph. But here, the interparticle spacing is so large that a particle will travel many diameters away from the wall before exchanging its rotational state in a collision. The Type A rotation rate increases monotonically from its value near the centre of the flow towards the large rotation rate applied at the wall. Exactly the opposite behaviour is apparent for the Type B boundary, which, by exerting no torque forces a local deficit in the rotation rate; there, the maximum rotation is observed in the centre of the channel and decreases steadily as the walls are approached.

Again, despite the similarity of the velocity and solid fraction profiles, the Type A and Type B temperature profiles in figure 6 are very different from one another, but very similar to the corresponding rotational velocity distribution (which may be an indication of the importance of particle rotation in temperature production). Here, the Type B profile shows a maximum in the centre of the channel and a minimum at either boundary. This can be explained by nearly the same reasoning as was used to explain the rotational velocity profiles. Remember that by forcing a particle's centre to assume exactly the wall's velocity, the Type B boundary eliminates any temperature in the x-direction and thus acts as a sink of granular temperature. In this light, the Type B temperature profile appears exactly as one would expect of a volume source of temperature with sinks at the boundaries. The effect is heightened because the granular temperature is anisotropic (particularly at small densities) with

its largest component acting in the x-direction† – which is precisely the component that is absorbed at the wall. On the other hand, the Type A profile shows the expected maxima near either boundary and a minimum in the centre of the channel, although, strangely, there is a slight temperature reduction directly next to the boundary. The reason for the reduction is not immediately clear. Remember, however, that the source of the large temperatures near Type A boundaries results from the conversion of the coherent rotational motion applied by the wall to granular temperature through subsequent collisions with other particles. Then, one might speculate that a reduced temperature could be observed near the wall for small solids concentrations because the subsequent collisions that lead to temperature generation occur some distance away from the wall.

Note that for $\bar{\nu} = 0.65$ the Type B boundary acts as a source of granular temperature, for $\bar{\nu} = 0.45$ the boundary acts as neither a source nor a sink, and for $\bar{\nu} = 0.15$ the boundary acts as a temperature sink. Different flow characteristics (in this case, the mean solid fraction, $\bar{\nu}$) will lead to different boundary behaviour. This indicates that one cannot separate the character of the boundary from the flow it bounds, but the two must be considered as a unified whole.

All of the above observations have common themes. The first is that the boundary exerts such a strong influence that it is not always possible to obtain uniform shear flows from flat wall-bounded systems. Secondly, the appearance of higher-shear-rate/lower-density/higher-temperature zones near the boundary seems to be interconnected and to be related to the range of free motion of the particles. When the density is large, such as for $\bar{\nu} = 0.65$ in figure 3, the particle motion is so restricted that whatever a particle picks up from the boundary is almost immediately exchanged in collisions with neighbouring particles. At such large concentrations, even the weak disturbance in the angular momentum distribution that is generated by the Type B boundary has noticeable consequences in the velocity and concentration profiles. By $\bar{\nu} = 0.15$, the effects of the boundary are so dispersed throughout the flow that even the Type A exhibits a uniform shear rate and density profile. This may be thought of as a kind of Knudsen number effect. For $\bar{\nu} = 0.65$, the mean free path of a particle is significantly smaller than a particle diameter, confining any disturbances introduced by the boundary to the immediate neighbourhood. At $\bar{\nu} = 0.15$, however, the mean free path is at least several particle diameters so that the wall effects may easily diffuse far from the wall.

The above also indicates that much happens over scales of particle diameters – at least near boundaries. This leads one to expect that there might be a strong effect of the ratio of the continuum scale, the wall spacing, to the microscopic scale, the particle diameter. To test this sensitivity, several simulations were run with varying wall separations of 10, 20, 40 and 80 particle radii. All of these were run with Type A boundaries as these demonstrate the strongest changes over particle scales. The results are presented in figure 7 (*a–c*), corresponding to average solid fractions of $\bar{\nu} =$

† This is a byproduct of the mechanisms that generate granular temperature (see, once again, the discussion in Campbell 1990). In addition to the collisional mechanism described previously, granular temperature can also be generated as a particle moves parallel to a velocity gradient; the difference in mean velocity between its initial and final positions appears as a random addition to the particle's velocity, but only makes a contribution in the direction perpendicular to the velocity gradient (in this case, the x-direction). Naturally, this will only make a significant contribution to the temperature at small densities when the particles move long distances between collisions. Campbell refers to this as 'Mode-2' temperature generation and it is used to explain large normal stress differences observed in granular flow at low densities (see Campbell & Gong 1986 and the stress measurements presented in the next section).

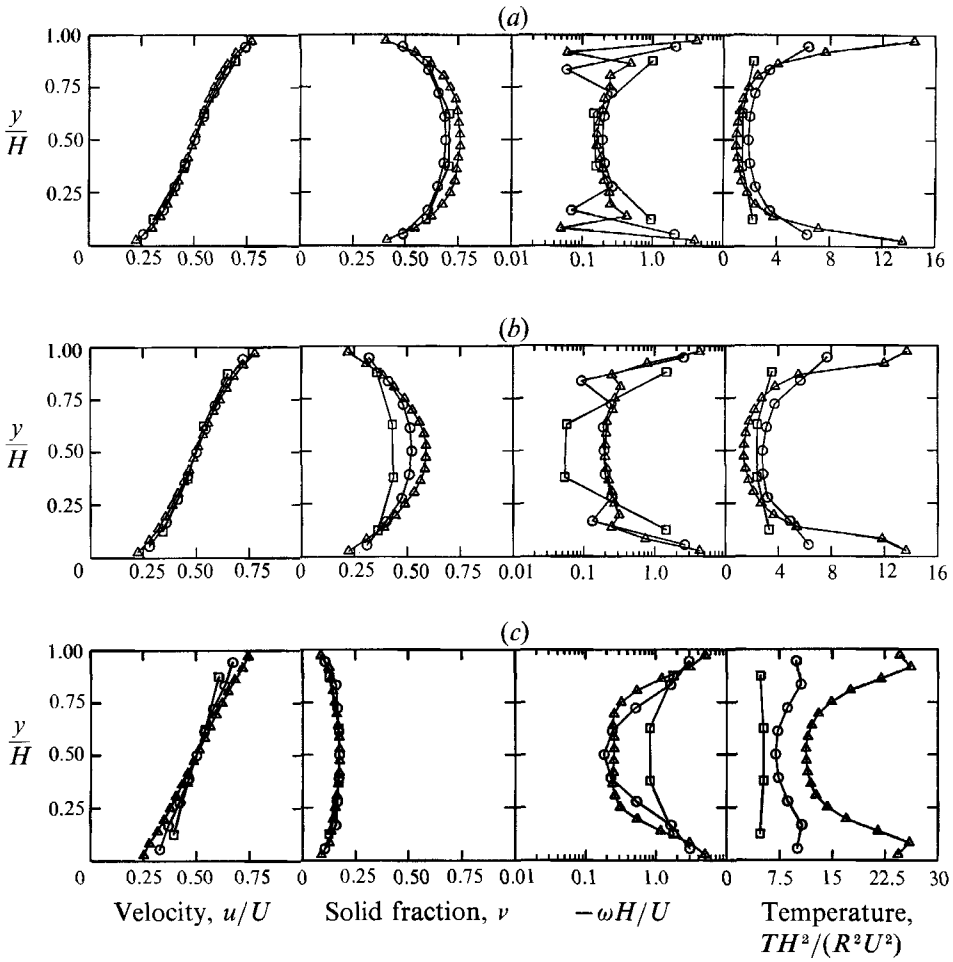

FIGURE 7. The effect of wall spacing on the flows with Type A boundaries: (*a*) $\bar{\nu} = 0.65$, (*b*) $\bar{\nu} = 0.45$, (*c*) $\bar{\nu} = 0.15$. □, $H/R = 10$; ○, $H/R = 20$; △, $H/R = 40$.

0.65, 0.45 and 0.15, respectively. Note that the $H/R = 80$ data have not been plotted to reduce the clutter on the figure. (Even so, it is hard to distinguish the various values of H/R within the figures and I must ask the reader to bear with me here.) However, when plotted in this scaling, the $H/R = 80$ data for $\bar{\nu} = 0.65$ and 0.45 nearly overlay the $H/R = 40$ data far from the boundaries. (It was on this basis that the spacing of $H/R = 40$ was chosen for the bulk of these simulations.) Overall, this is encouraging as it indicates that, beyond a certain spacing, the behaviour of the material far from the walls is determined by the continuum scales of the wall velocity and separation distance; if this were not so, the rheological properties of the system would not scale in any way with the imposed shear rate U/H. But, many events, such as the rotational exchange illustrated in figure 4 (*b*) and its corresponding temperature generation, occur on scales of the order of a particle diameter. As these effects were apparent for all gap widths, and, as the vertical coordinate is normalized by the continuum scale, H, instead of the microscopic scale, R, one can never expect the profiles to overlap in the immediate neighbourhood of the boundary. It is apparent from all three figures that the $H/R = 10$ separation is dominated by the effects at the wall. This may best be seen by examining the rotational velocity distributions. For

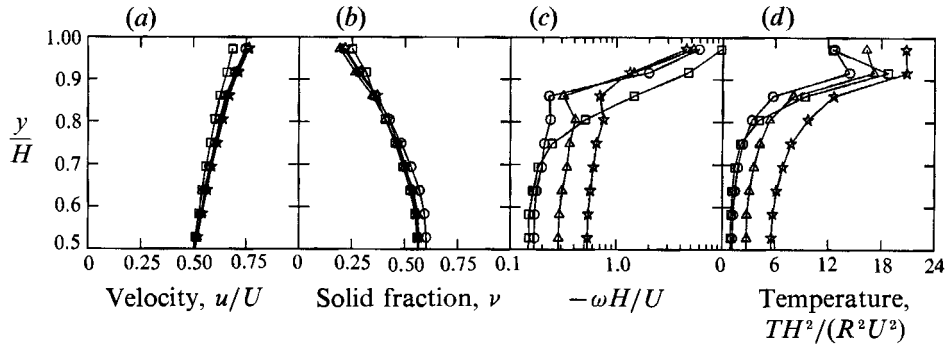

FIGURE 8. The effect of the particle surface friction coefficient, μ, on Type A boundary flows. In all cases, $\mu_w = 1.0$. Note that, in order to show the boundary more clearly, only the top half of each distribution has been plotted. □, $\mu = 0.1$; ○, $\mu = 0.25$; △, $\mu = 0.5$; ☆, $\mu = \infty$.

the two higher concentration plots shown in figures 7(*a*) and 7(*b*), the jagged behaviour near the boundaries (the results of the mechanism illustrated in figure 4*b*) is missing from the curves. Instead, the $H/R = 10$ points just show a slightly elevated rotation rate near the walls. This could also explain the reduced granular temperature in the vicinity of the walls since a smaller rotational velocity implies a smaller conversion of rotational velocity into granular temperature. At larger separations, the higher density plots assume the more characteristic forms that were described above. The sole exception is the $\bar{\nu} = 0.15$ case, for which it is apparent that, due to the large mean free path of the particles at such a small density, the wall effect extends far into the flow. Notice that there is a general trend of increasing rotation rates and granular temperatures as the spacing is increased. With the exception of $\bar{\nu} = 0.15$, this process halted by $H/R = 40$ as those measurements matched the corresponding $H/R = 80$ results. That this process continued for the $\bar{\nu} = 0.15$ case is clearly the result of the diffusion of these properties away from the wall by the enhanced free motion of the particles.

It may seem that the Type A condition, with its effectively infinite friction coefficient, is a bit unrealistic and, therefore, it may be prudent to examine the effects of friction. This is illustrated in figures 8 and 9, which show the results of what are essentially Type A calculations except that they possess finite values of the surface friction coefficient. In the former, the particle–particle surface friction coefficient, μ, is varied, while the particle–wall friction coefficient, μ_w, is held fixed at $\mu_w = 1.0$; and in the latter, the particle–particle coefficient is held fixed at $\mu = 0.5$, while μ_w is varied. All of these studies were performed at an average solid fraction of $\bar{\nu} = 0.45$. Physically, varying the particle friction while holding the wall friction coefficient fixed varies the rate at which rotational velocity is exchanged during particle–particle collisions. Naturally, the curves show the expected top to bottom symmetry, and, to reduce the clutter on the figures, only the data from the top half of the control volume is plotted. Notice that, surprisingly, the velocity and solid fraction profiles in figure 8 appear to be relatively independent of the surface friction. However, the rotational velocity profiles, shown in figure 8(*c*), show a strong effect. Most obvious is that, except right next to the wall, the larger the friction coefficient, the larger the mean rotational velocity. But this behaviour is reversed in the immediate vicinity of the wall as the larger the surface friction, the more resistance the surrounding particles bring to bear against the rapid rotation induced by a wall collision. Note also that all of the profiles except that corresponding to $\mu = 0.1$ show, to varying

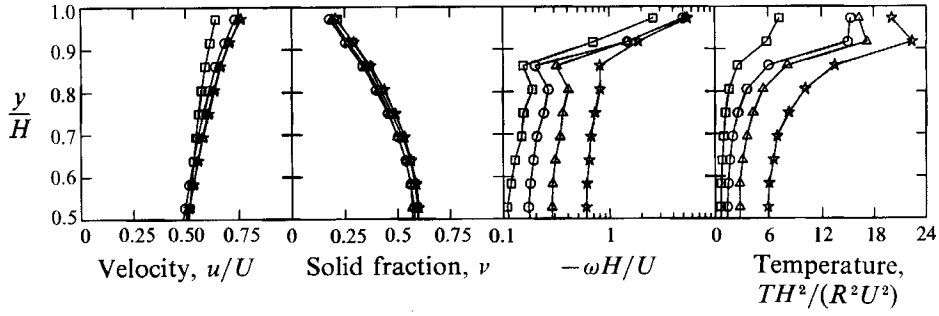

FIGURE 9. The effect of the wall surface friction coefficient, μ_w, on Type A boundary flows. In all cases, $\mu_w = 0.5$. Note that, in order to show the boundary more clearly, only the top half of each distribution has been plotted. □, $\mu_w = 0.5$; ○, $\mu_w = 0.75$; △, $\mu_w = 1.0$; ☆, $\mu_w = \infty$.

degrees, the jagged shape near the wall that is characteristic of the rotational exchange mechanism illustrated in figure 4(*b*). The $\mu = 0.1$ profile shows a gradual variation near the wall that is characteristic of a more diffusive type of rotational velocity transport (i.e. is similar to that for the $\bar{\nu} = 0.15$ distribution plotted in figure 6), presumably because the coupling between the particle surfaces is so weak. Large variations are also apparent in the granular temperature profiles. Note that, as changing the particle surface friction changes the coupling between the particle surfaces, such action might be interpreted as changing the internal conversion of the coherent rotational velocity into granular temperature. This process may be seen in figure 8, in which the granular temperature is largest for the largest values of the surface friction and generally decreases as the surface friction is reduced, clearly showing the importance of the rotational exchange at the boundary in determining the overall granular temperature distributions in the flow. (As friction introduces another dissipation mechanism, one would generally expect, in the absence of such strong boundary effects, lower granular temperatures for larger surface frictions.) An interesting feature is that the coefficient of particle surface friction changes the temperature gradient at the wall and, thus, appears to govern whether the wall acts as a local source or sink of granular temperature. For the smaller values of the friction coefficient, there is a negative temperature gradient immediately approaching the wall, implying that there is conduction of granular temperature into the boundary; this gradient becomes smaller as the surface friction is increased until, for infinite friction, the gradient has nearly disappeared and the wall appears to be an insulator. (However, figure 5 shows that, if the wall surface friction is also infinite, the wall acts as a source of granular temperature.) But one should be careful about making such attributions as these effects are confined to within a particle diameter of the wall; further away, on continuum scales, the temperature decreases steadily toward the channel centre, indicating that, globally, all the boundaries are acting as sources of granular temperature.

Further insight can be found from figure 9 which shows the effect of varying the particle–wall friction coefficient, μ_w, while the particle–particle friction coefficient, μ, is held fixed. Once again, very little change is observed in the velocity and solid fraction profiles; the only significant velocity effect occurs for the smallest friction coefficient, $\mu_w = 0.5$, for which the coupling between the material and the wall is so weak that only a small velocity gradient can be generated within the flow. (In fact, the simulation would not shear and exhibited essentially solid behaviour for much smaller μ_w.) Furthermore, the larger the friction coefficient the larger the rotational

velocity that is generated within the centre of the flow. At first glance, it may appear that changing μ_w changes the rotational velocity in the centre of the channel, with little effect on the rotation at the wall; however, remember that this is plotted on a log scale, so that the apparently small difference in rotation rate at the wall is consistent with the apparently larger variation towards the centre of the channel. More interesting is the variation in the granular temperature profiles. Again, the larger the friction coefficient. the larger the magnitude of the granular temperature. However, for the smaller values of μ_w, the temperature gradients indicate that the wall is locally acting as a source of granular temperature, while, for the larger μ_w, the wall is locally acting as a temperature sink (but, again, only on microscopic scales). Presumably, this represents the interplay between the collisional and rotational sources of the granular temperature.

4. Internal stress distribution

There are two mechanisms of internal momentum transport by which stress is transmitted through a granular material. The first, or streaming mode, denoted τ_s, reflects the momentum that is carried by particles as they move through the bulk material following their random velocity. In appearance, the streaming stress tensor is exactly the same as the Reynolds' stress tensor in turbulent flow:

$$\boldsymbol{\tau}_s = -\rho_p \nu \langle \boldsymbol{u}'\boldsymbol{u}' \rangle \tag{3.1}$$

where $\langle \boldsymbol{u}'\boldsymbol{u}' \rangle$ is the average of the dyadic product of the fluctuating velocity vectors, $\boldsymbol{u}'$. Obviously, the magnitude of the streaming stresses should be related in some way to the magnitude of the granular temperature. Note that $\boldsymbol{\tau}_s$ is necessarily symmetric. Also, when two particles collide, momentum is transferred from the centre of one particle to the other. This is the collisional mode of momentum transfer and results in the collisional stress tensor, $\boldsymbol{\tau}_c$:

$$\boldsymbol{\tau}_c = 2R\langle \boldsymbol{J}\boldsymbol{k} \rangle \eta, \tag{3.2}$$

where $\langle \boldsymbol{J}\boldsymbol{k} \rangle$ is the average of the dyadic product of $\boldsymbol{J}$, the vector impulse exerted by a collision, $\boldsymbol{k}$ is the unit vector pointing along the line connecting the particle centres at the time of collision and η is the collision rate per unit volume. This reflects the fact that every collision causes the transport of momentum, $\boldsymbol{J}$, a distance $2R$ in the direction $\boldsymbol{k}$ between the particle centres. Note that, as part of the impulse results from the frictional coupling of the particle surfaces, $\boldsymbol{J}$ need not point in the same direction as $\boldsymbol{k}$, so that the collisional contribution may possibly make asymmetric contributions to the stress tensor. Obviously, the collisional mode will be more important at large density where a particle cannot move far between collisions and the streaming mode is dominant at low densities where collisions are infrequent and particle motion is less restricted. The total stress tensor, $\boldsymbol{\tau}$, is found by summing these two contributions. For more information on how the stress tensor is found, the reader is referred to Campbell & Gong (1986). Here, as there, the plotted stresses are scaled by dividing the actual stresses by $\rho_p R^2 (U/H)^2$, following the scaling originally found for shear flows by Bagnold (1954). Note that the plots show absolute value of the stresses; in all cases, the normal stresses are negative and the shear stresses are positive.

Previous computer simulation studies that measured the stress tensor in granular flows (e.g. Campbell & Gong 1986; Campbell 1989) have purposely chosen conditions for which the state of stress is uniform across the control volume. In this study,

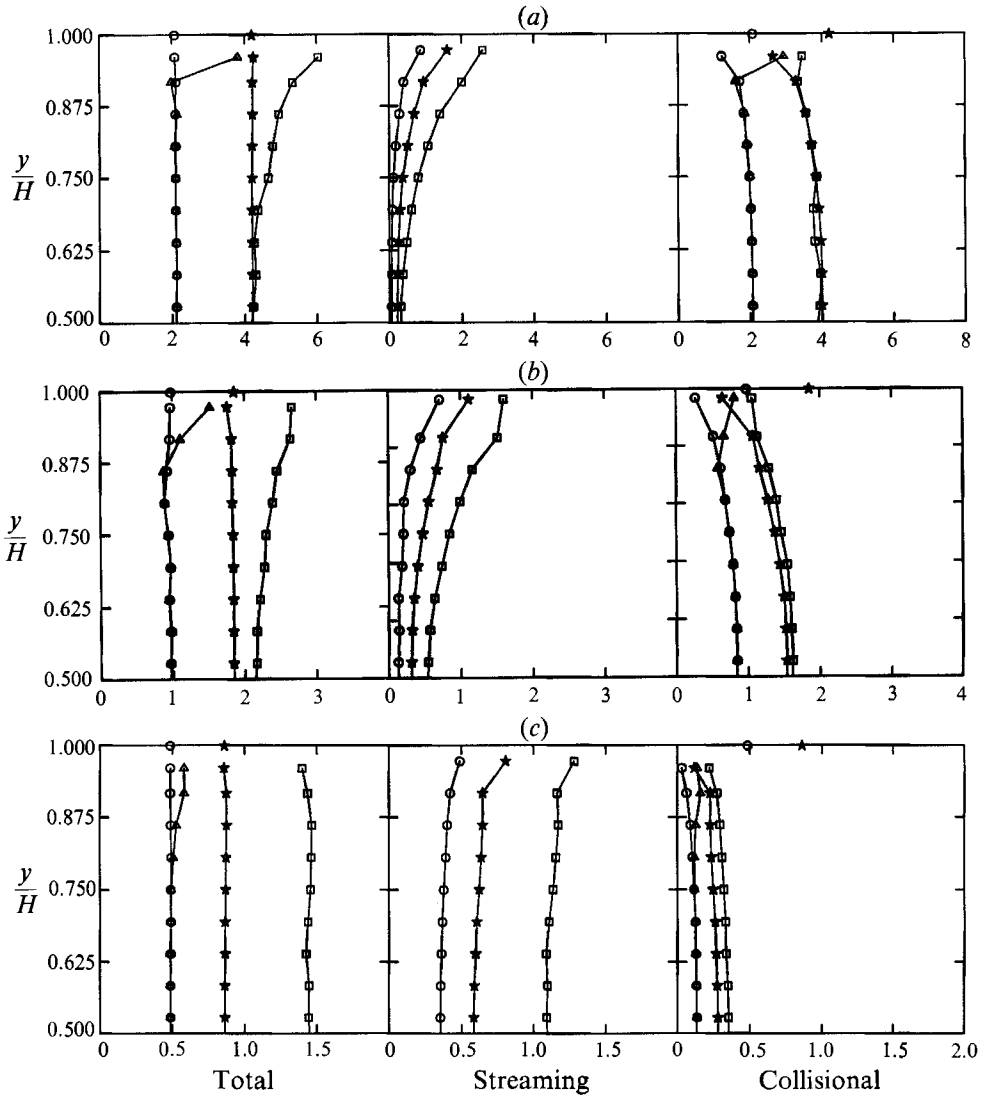

FIGURE 10. The distribution of internal stress across the channel for the Type A boundary: (*a*) $\bar{\nu} = 0.65$, (*b*) $\bar{\nu} = 0.45$, (*c*) $\bar{\nu} = 0.15$. Note that, in order to show the boundary region more clearly, only the top half of each distribution has been plotted. □, τ_{xx}; ○, τ_{xy}; △, τ_{yx}; ☆, τ_{yy}.

however, the boundaries will induce non-uniformities in stress. To observe the non-uniformities, the distribution of stress across the channel was found by dividing the control volume into strips parallel to the wall and averaging the state of stress within the strips. For the streaming stresses, this procedure is exactly that used to average the velocity and the other continuum properties. But for the collisional stresses, there is the possibility that the colliding particles may be in different strips; thus, the fraction of $\langle \boldsymbol{Jk} \rangle$ attributed to each strip is weighted by the transport distance through that strip.

There are some fine points that must be taken into account in order to properly sample the stresses near the walls. Because the particles have finite size, the centre of a particle cannot come closer to the wall than the radius of the smallest particle

in the system. In a collision with the wall, forces are applied to a particle in the x- and y-directions. These impulses are conveyed along a vertical line connecting the centre of the particle with the wall. Thus, a collision results in the transport of x- and y-direction momentum along a line segment one particle radius in length and oriented in the y-direction. Consequently, the only stresses transmitted within one particle radius of the wall are the τ_{xy} and τ_{yy} collisional stresses applied at the wall. Thus, one might consider that the wall has a range of influence extending one particle radius outwards into the flow. No particle centre extends into that region nor can a contact point between two colliding particles lie therein. Thus, in that zone, the only stresses are the τ_{xy} and τ_{yy} stresses applied by the wall, and any τ_{xx} and τ_{yx} components can only be generated further outward in the flow as a response to the forces applied at the boundaries. (However, the τ_{xx} and τ_{yx} stresses show significant variation across the control volume, indicating a strong boundary influence.) The values corresponding to the stresses applied at the wall are plotted as points lying on the upper boundary. As these stresses are only transmitted by collisions with the wall, they only appear in the plot of the total and collisional stresses. In order to properly evaluate the stresses in the averaging strip nearest the wall, the volume associated with the wall-dominated zone (i.e. a strip one particle radius wide) must be excluded from the averaging volume.

Figures 10 and 11 show the internal distribution of stress for the Type A and Type B boundary conditions that correspond to the results shown in figures 3, 5 and 6. Here, the total stresses are plotted along with the collisional and streaming contributions. (As $\boldsymbol{\tau}_s$ is necessarily symmetric, only the τ_{xy} and not the τ_{yx} component is plotted in that frame.) Note that the complete stress levels for the Type B condition are significantly larger than for the Type A, illustrating that a difference in boundary condition can account for the difference between the stresses measured by Hanes & Inman (1985) and Savage & Sayed (1984). Note also that, at the rather large density ($\bar{\nu} = 0.65$) shown in figures 10(a) and 11(a), the collisional mode of momentum transport is much more important than the streaming, but for the lowest average solid fraction, $\bar{\nu} = 0.15$, plotted in figures 10(c) and 11(c), the streaming stresses dominate. As would be expected, even in the higher $\bar{\nu}$ plots, the streaming stresses are noticeably larger within the lower density and high granular temperature regions near the boundaries, and are accompanied by correspondingly smaller collisional stresses. Furthermore, in the Couette flow configuration, the τ_{xx} and τ_{yx} stresses cannot be applied by the boundaries; hence, these stresses are self-equilibrated and the values they assume are completely determined by the flow conditions. Also, the τ_{xy} and τ_{yy} stress exerted at one wall can only be balanced on the opposite wall. Hence, these two stresses must be uniform across the channel and equal to the values applied at the wall. Finally, note that normal stress differences, $\tau_{xx} > \tau_{yy}$, are present in the flow, reflecting the anisotropy in the granular temperature. These are similar to those observed by Campbell & Gong (1986). The normal stress differences are much more noticeable in the low density, $\bar{\nu} = 0.15$ plots, but can also be seen in the low density regions near the walls of the $\bar{\nu} = 0.45$ and $\bar{\nu} = 0.65$ plots.

In the few layers nearest the walls of the Type A boundary distribution plotted in figure 10, the stress tensor is asymmetric, i.e. $\tau_{xy} \neq \tau_{yx}$. This is a bit surprising since, in elementary continuum mechanics, there is a simple proof that the stress tensor must be symmetric. The proof involves relating the angular momentum change of the bulk material lying within a contour to the contour integral of the stress; on shrinking the contour, the moment of inertia disappears faster than the contour

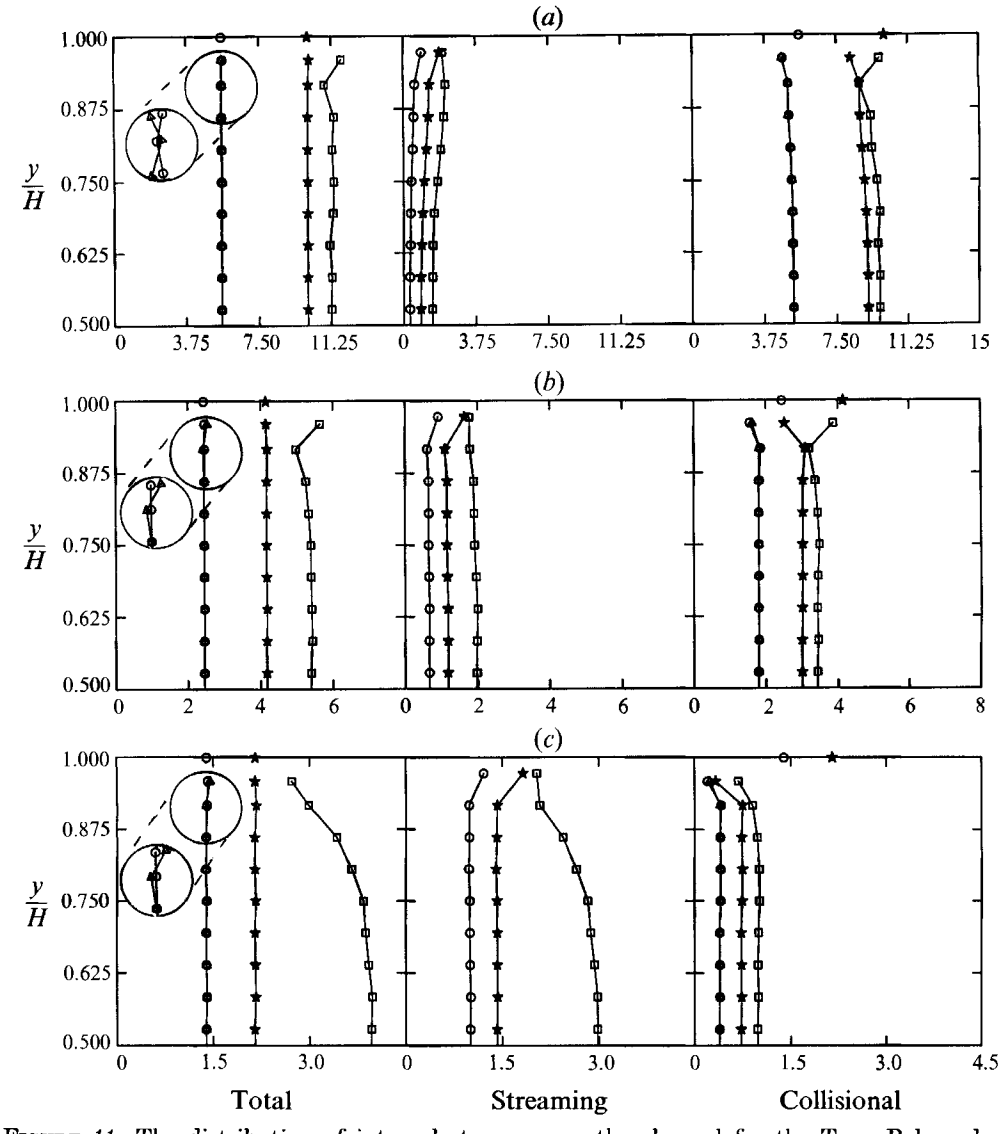

FIGURE 11. The distribution of internal stress across the channel for the Type B boundary: (*a*) $\bar{\nu} = 0.65$, (*b*) $\bar{\nu} = 0.45$, (*c*) $\bar{\nu} = 0.15$. Note that, in order to show the boundary region more clearly, only the top half of each distribution has been plotted and the horizontal scale of the points nearest the wall has been expanded in bubbles to make the asymmetries more apparent. Symbols as figure 10.

integral, implying that the stress tensor is symmetric. This argument breaks down for a granular material as, for a continuum model to be valid, any such contour must contain several particles and, certainly, such a contour cannot be shrunk smaller than a particle. In this light, it is reasonable to associate the asymmetry in the stress tensor with torques on the particles. Consider first the $\bar{\nu} = 0.65$ data shown in figure 10(*a*). Now, the wall exerts a τ_{xy} stress but no τ_{yx} stress, indicating that the particles receive a tremendous clockwise torque at the wall. But, in the layer nearest the boundaries, $\tau_{yx} > \tau_{xy}$, indicating that the granular mass exerts a counterclockwise torque to resist the clockwise torque exerted by the wall. In the second layer away

from the wall, the situation has reversed itself and $\tau_{yx} < \tau_{xy}$, indicating that the particles in this region experience a clockwise torque. Finally, in the next layer out, although it is barely perceptible, $\tau_{yx} > \tau_{xy}$, indicating, once again, that a counterclockwise torque is being exerted in this region. Note that this pattern follows the jagged nature of the $-\omega I I/U$ curve shown in figure 3, reflecting the rotational exchange mechanism illustrated in figure 4(*b*). Now, for the $\bar{\nu} = 0.15$ data shown in figure 10(*c*), $\tau_{yx} > \tau_{xy}$ in all of the first four layers closest to the wall, implying that the material is exerting counterclockwise torques throughout this region to resist the large clockwise torque applied at the wall. As previously discussed, this reflects the fact that, at such a low concentration, a particle, following a wall collision, is likely to travel a long way out into the flow before it collides again. In the $\bar{\nu} = 0.65$ case shown in figure 10(*a*), the particle has almost no freedom of motion and the countertorque applied by the material is confined to the region immediately adjacent to the wall, leading to rotational exchange by the mechanism illustrated in figure 4(*b*). In the $\bar{\nu} = 0.15$ case plotted in figure 10(*c*), the countertorque applied by the material is distributed over a wider region. Note that this corresponds exactly to the rotational velocity distribution shown in figure 6, which shows a gradual decrease in rotation rate, from the large rotations applied at the wall to the much smaller values seen near the centre of the channel. The stress distribution for $\bar{\nu} = 0.45$, shown in figure 10(*b*), is a compromise between these two cases. There, in the two layers nearest the wall, $\tau_{xy} > \tau_{yx}$ (counterclockwise torque), but then the two stresses reverse roles in the third layer out, where $\tau_{yx} > \tau_{xy}$. Note that this is, once again, consistent with the rotational distribution shown in figure 5, which does not show the jaggedness associated with the rotational exchange mechanism of figure 4(*b*) until the third layer out. This behaviour may be understood by noting, from the corresponding solid fraction distribution shown in figure 5, that the density is significantly reduced in the two layers nearest the wall and, consequently, one might expect low-density behaviour similar to that shown in figure 10(*c*); high-density behaviour, similar to that shown in figure 10(*a*), appears in the higher-density regions near the centre.

Similar asymmetries, though much less dramatic, are also apparent for the Type B boundary results shown in figure 11. In order to make the asymmetries apparent at all, the horizontal scales of the three points nearest the wall have been expanded in a bubble within the total stress figure. This is an indication that, by exerting no torque, the Type B boundary alters, ever so slightly, the internal distribution of angular momentum.

The presence of asymmetric stresses poses somewhat of a quandary as they imply that there are unbalanced torques on the particles and, if there is an unbalanced torque, the angular velocity should be continually accelerating. Yet these are steady flows so the average angular velocity must be constant with respect to time, which requires that the torques that are implied by the asymmetric stress tensor must somehow be balanced. This indicates that the stress tensor alone is inadequate to explain the transport of angular momentum within the granular mass. It is easy to see that, in the process of averaging the microscopic details of the collisions to obtain the macroscopic stress tensor, much of the information about the moments has been lost; for example, there are continuous ranges of collisions exerting infinitely many different torques that will yield the same dyadic product, $\boldsymbol{Jk}$, and, consequently, make the same contribution to the stress tensor. In a macroscopic continuum sense, then, the transport of angular momentum is independent of the transport of linear momentum even though, on the microscopic level, both result from the same

conditions. Thus, another field variable is required to describe the transport of angular momentum. The 'couple stress tensor' is a direct analogue to the Cauchy stress tensor and reflects the transport of angular momentum both by streaming and collisional action. The streaming portion of the couple stress tensor, $\boldsymbol{M}_s$, is given by

$$\boldsymbol{M}_s = -\rho_p \beta \nu R^2 \langle \boldsymbol{u}'\boldsymbol{\omega}' \rangle, \tag{3.3}$$

where $\rho_p \beta \nu R^2$ may be thought of as the particle moment of inertia per unit volume and $\langle \boldsymbol{u}'\boldsymbol{\omega}' \rangle$ is the average of the dyadic product of the fluctuating linear and angular velocities. Also, each collision causes a transport of angular momentum $R\boldsymbol{J}\times\boldsymbol{k}$, a distance $2R$ (between the particle centres) in the $\boldsymbol{k}$-direction. Thus, the collisional contribution to the couple stress tensor is given by

$$\boldsymbol{M}_c = 2R^2 \langle \boldsymbol{J}\times\boldsymbol{k}\boldsymbol{k} \rangle \eta, \tag{3.4}$$

where, once again, η is the collision rate per unit volume. The complete couple stress tensor is found by summing the streaming and collisional contributions. Each component, M_{ij}, of the couple stress tensor may be read as 'the surface torque component in the i direction exerted on a surface with outward pointing normal unit vector in the j direction'. In two-dimensions, where the only permitted rotation is about an axis oriented in the z-direction, there are only two non-zero couple stress components, M_{zx} and M_{zy}, representing the transmission of z-direction angular momentum in the x- and y-directions respectively. Figure 12(a, b) shows the collisional and streaming contributions to the couple stress tensor for a Type A boundary at a high density, $\bar{\nu} = 0.65$. The couple stress data which are to follow have all been scaled by dividing by $\rho_p R^3 (U/H)^2$. The surprising thing about this figure is that the streaming mechanism makes the largest contribution to the angular momentum transport, even at such a large concentration. (And, of course, the collisional contribution is even smaller as $\bar{\nu}$ is further reduced.)

Performing an angular momentum balance on a control volume in steady flow, one obtains the expression

$$M_{ij,j} - \epsilon_{ijk}\tau_{jk} = 0. \tag{3.5}$$

Thus, the asymmetry in the stress tensor is balanced by the divergence of the couple stress tensor. In two dimensions, the particles are forced to rotate within the plane, and, as in Couette flow all gradients are in the y-direction, this expression becomes

$$M_{zy,y} + (\tau_{yx} - \tau_{xy}) = 0, \tag{3.6}$$

where z is the coordinate direction out of the plane of motion. Thus, even though there will be an M_{zx} component generated in the granular mass, it represents self-equilibrated torques and is not dynamically important.

Figures 13 and 14 show the distribution of couple stress across the channel for the Type A and Type B boundaries, respectively. Also plotted for comparison are the corresponding rotational velocity distributions. Here, unlike the Cauchy stresses plotted in figures 10 and 11, the actual (and not the absolute) values of the couple stresses are shown since the components change sign across the control volume. The points on the top and bottom edges of the plot represent the torques applied by the walls. Both M_{zx} and M_{zy} components are shown even though (3.6) indicates that the only dynamically important component is M_{zy}. (Remember, however, that it is the gradients of M_{zy}, and not its actual numerical values, that are important in determining the rotational state of the particles.) Furthermore, the torque applied at the boundary only contributes to the M_{zy} component.

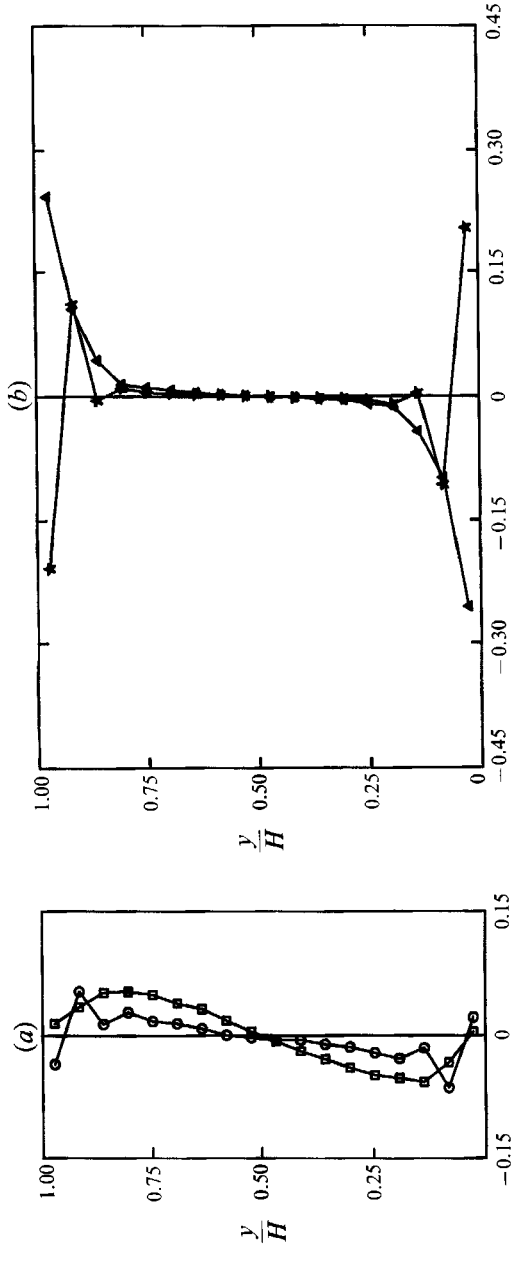

FIGURE 12. (*a*) The collisional contribution to the couple stress. The wall corrections have been excluded from these data. □, M_{xx}; ○, M_{xy}. (*b*) The streaming contribution to the couple stress. ▲, M_{xx}; ★, M_{xy}. $\bar{\nu} = 0.65$, Type A boundary. Note that the horizontal scales for the plots are different.

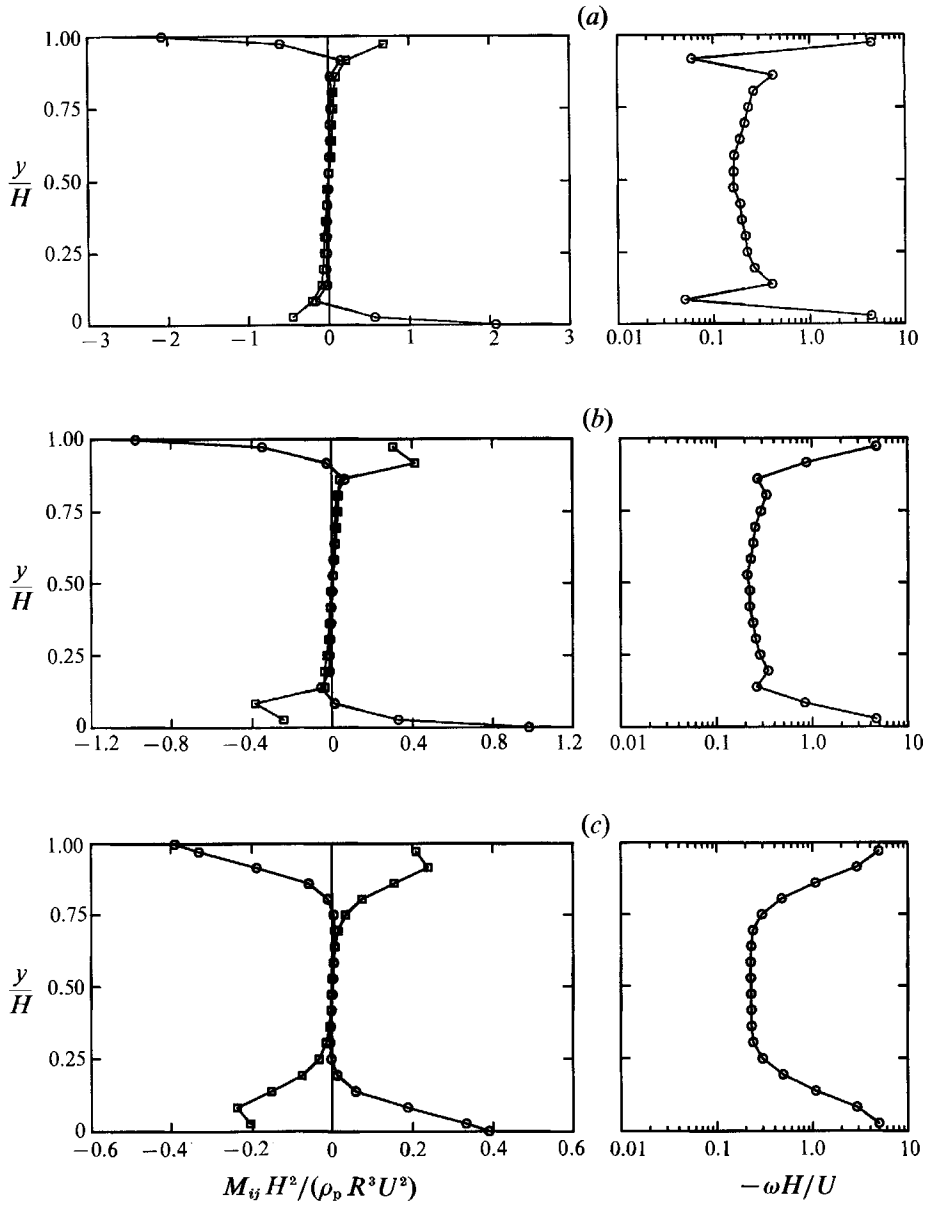

FIGURE 13. The distribution of couple stress across the channel for the Type A boundary: (*a*) $\bar{\nu} = 0.65$, (*b*) $\bar{\nu} = 0.45$, (*c*) $\bar{\nu} = 0.15$. Also plotted are the corresponding rotational velocity distributions. Note that the horizontal scales for the various plots are different. □, M_{zx}; ○, M_{zy}.

Figure 13(*a–c*) shows the distribution of couple stress across the channel for $\bar{\nu} = 0.65$, 0.45 and 0.15, respectively, all derived with Type A boundaries. These correspond to the stress tensor measurements shown in figure 10. Note, first, that the larger the density, the larger the absolute values of the imparted couple stresses. Also, note that the top wall imparts a negative value of M_{zy} while the bottom wall exerts a positive value. This may seem strange to the uninitiated as both boundaries exert negative (clockwise) torques on the particles. However, the outward-pointing normal unit vector changes sign between the top and bottom wall and, consequently,

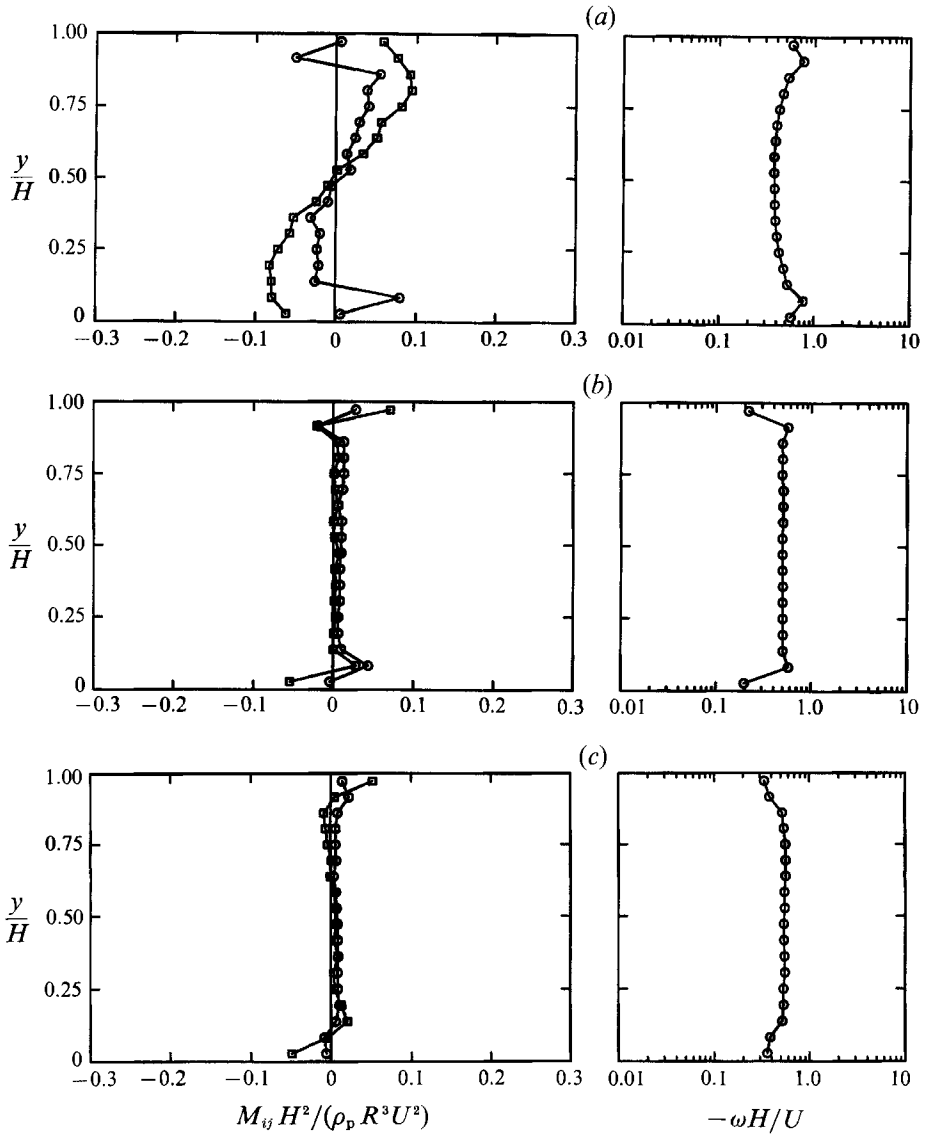

FIGURE 14. The distribution of couple stress across the channel for the Type B boundary: (*a*) $\bar{\nu} = 0.65$, (*b*) $\bar{\nu} = 0.45$, (*c*) $\bar{\nu} = 0.15$. Also plotted are the corresponding rotational velocity distributions. □, M_{zx}; ○, M_{zy}.

the sign of M_{zy} must also change in order to represent the application of the same torque by the lower wall. Furthermore, both components of couple stress go nearly to zero in the centre of the channel, indicating that couple stresses are only significant players near the boundaries. Perhaps the most important point to be gained from examining these figures is that the couple stress follows the behaviour of the rotational velocity distribution; i.e. the jags in the rotational velocity distributions correspond to sign changes in M_{zy}. At the same time, the couple stress mirrors the asymmetry in the stress tensor. Also, the reader can see behaviour consistent with (3.6), although it is impossible to make a quantitative comparison as, with such rapid changes between neighbouring points, the gradient of M_{zy} cannot be accurately determined. But, remember that these points represent averages over

strips that are only slightly larger than a particle diameter wide and that such radical changes over such small scales lie at or beyond the limit of applicability of continuum theories.

Figure 14 shows the corresponding couple stress distribution for the Type B boundary. As these boundaries exert no torque, the magnitudes of the couple stresses that are generated are significantly reduced. Still, it is apparent that the boundary does induce perturbations in the couple stresses within its immediate vicinity. Notice that the couple stress near a Type B boundary is positive near the top wall and negative near the bottom, reflecting that a counterclockwise torque is being generated at both boundaries. This is exactly opposite to the behaviour of the Type A boundary, for which there are large negative couple stresses at the upper wall and positive couple stresses at the lower wall, due to the large clockwise torques imposed at each boundary. Consequently, the natural clockwise rotation of the particle is inhibited near Type B boundaries. This is a reflection of the fact that, even by inducing no torque of its own, the Type B boundary disturbs the natural distribution of angular momentum in the flow.

5. Conclusions

In any fluid-like flow, the boundaries are extremely important in that they, with the possible collaboration of body forces, ultimately drive the motion. This paper has studied the effects of two different flat-wall boundaries on Couette flows of two-dimensional granular materials. The Type A boundary assumes that, on contact with a wall, there is no-slip between the particle surface and the wall, and, for the Type B boundary condition, there is no-slip between the particle centre and the wall. (Historically, these two boundary conditions are linked to the work of Campbell & Brennen 1985*a*, which provided the impetus for this current study.) The two boundary conditions are artificial in that the Type A boundary assumes an infinite friction coefficient between a particle and the wall (although, all the features of the Type A boundary are present in flows with more realistic frictional interactions) and that there is no way to physically realize a type B boundary at all. Nonetheless, they are important to study as they represent extremes of the manner in which a boundary can apply torque to the flowing particles. By allowing no slip between the particle surface and the wall, the Type A condition applies the maximum possible torque to a colliding particle and the Type B condition provides no torque at all.

The most important result of this paper is that the way in which a boundary transmits torque to a particle can have a significant influence on the overall flow behaviour. One byproduct of the Type A boundary is large local granular temperature generation. This is a direct result of the nature of the boundary as the coherent rotational velocity applied by a wall collision is converted, on subsequent collisions, into random velocities. But both boundary types, by disturbing the natural distribution of angular momentum within the material, lead to the generation of asymmetric stresses and couple stresses in the immediate neighbourhood, even though their effects may be insignificant further away. An important observation is that frictional materials need to be modelled as polar materials, at least in the neighbourhood of boundaries and that one factor that characterizes a boundary is the way it transmits couple stress to the flowing material.

Many of the interesting observations in these results occur over lengthscales of the order of a particle diameter. In fact, the dramatic differences between the Type A and Type B boundaries are caused by moving the point at which the impulse from

a boundary collision is applied one particle radius further away from the wall (a distance that should be insignificant from a continuum point of view). The importance of particle scales is also apparent in the rotational velocity, stress tensor asymmetries and the couple stress distributions as a result of the rotational transfer mechanism illustrated in figure 4(*b*). Furthermore, this mechanism is extremely important in converting the coherent rotational velocity administered at the wall into granular temperature and consequently cannot be ignored if the physics of the boundary are to be modelled exactly.† As so much of importance occurs over such small lengthscales, it is questionable whether boundary phenomena can be adequately modelled by continuum mechanical approaches. But any final determination will have to wait for the development of theoretical models that can accurately incorporate significant particle friction.

Finally, these results indicate that the characteristics of the boundary cannot be specified independently of the flow that it bounds. Different flow conditions, e.g. different mean particle concentrations, result in very different behaviour from what, physically, is the same boundary. Hence, the flow problem cannot be considered separate from the boundary, and the two must be solved together as a unified whole.

This study was supported by the National Science Foundation under grants MEA-8352513 and CTS-8907776, with additional funding provided by the International Fine Particle Research Institute, IBM and Sun Microsystems for which the author is extremely grateful. The author would like to thank Ailing Gong for her participation in the early portions of this study and Professor J. D. Goddard for insights into couple stresses. Additional thanks are due to Holly Campbell for proofreading the manuscript and to Ian and Sean for standing so tall.

REFERENCES

Ahn, H., Brennen, C. E. & Sabersky, R. H. 1991 Measurement of the velocity, velocity fluctuation, density and stresses for chute flows of granular material. *Trans. ASME* E: *J. Appl. Mech.* **58**, 792–803.

Augenstein, D. A. & Hogg, R. 1978 An experimental study of the flow of dry powders over inclined surfaces. *Powder Tech.* **19**, 205–215.

Bagnold, R. A. 1954 Experiments on a gravity-free dispersion of large solid particles in a Newtonian fluid under shear. *Proc. R. Soc. Lond.* A **225**, 49–63.

Bailard, J. 1978 An experimental study of granular-fluid flow. PhD dissertation, University of California, San Diego.

Campbell, C. S. 1982 Shear flows of granular materials. PhD thesis; and *Rep.* E-200.7. Division of Engineering and Applied Science, California Institute of Technology.

Campbell, C. S. 1988 Boundary interactions for two-dimensional granular flows: asymmetric stresses and couple stresses. In *Micromechanics of Granular Materials* (ed. M. Satake & J. T. Jenkins), pp. 163–174. Elsevier.

Campbell, C. S. 1989 The stress tensor for simple shear flows of a granular material. *J. Fluid Mech.* **203**, 449–473.

Campbell, C. S. 1990 Rapid granular flows. *Ann. Rev. Fluid Mech.* **22**, 57–92.

Campbell, C. S. 1993 Boundary interactions for two-dimensional granular flows. Part 2. Roughened boundaries. *J. Fluid Mech.* **247**, 137–156.

† As the particle diameter becomes an important lengthscale near boundaries, significant changes in the flow behaviour might be expected if many particle sizes were present. It is not clear what all of these might be but, certainly, some strong change might occur in the rotational transfer process described by figure 4(*b*) as different sized particles will undergo rotational reversal at different distances from the wall.

CAMPBELL, C. S. & BRENNEN, C. E. 1985*a* Computer simulation of granular shear flows. *J. Fluid Mech.* **151**, 167–188.

CAMPBELL, C. S. & BRENNEN, C. E. 1985*b* Chute flows of granular material: some computer simulations. *Trans. ASME* E: *J. Appl. Mech.* **52**, 172–178.

CAMPBELL, C. S. & GONG, A. 1986 The stress tensor in a two-dimensional granular shear flow. *J. Fluid Mech.* **164**, 107–125.

CRAIG, K., BUCKHOLTZ, R. H. & DOMOTO, G. 1987 The effects of shear surface boundaries on stresses for the rapid shear of dry powers. *Trans. ASME J. Tribol.* **109**, 232–237.

DRAKE, T. G. & SHREVE, R. L. 1986 High speed motion pictures of nearly steady, uniform, two-dimensional, inertial flows of granular material. *J. Rheol.* **30**, 981–993.

HANES, D. M. & INMAN, D. L. 1985 Observations of rapidly flowing granular fluid flow. *J. Fluid Mech.* **150**, 357–380.

HANES, D. M., JENKINS, J. T. & RICHMAN, M. W. 1988 The thickness of steady plane shear flows of circular disks driven by identical boundaries. *Trans. ASME* E: *J. Appl. Mech.* **55**, 969–974.

HUI, K., HAFF, P. K., UNGAR, J. E. & JACKSON, R. 1984 Boundary conditions for high shear grain flows. *J. Fluid Mech.* **145**, 223–233.

ISHIDA, M. & SHIRAI, T. 1979 Velocity distributions in the flow of solid particles in an inclined open channel. *J. Chem. Engng Japan* **12**, 46–50.

JENKINS, J. T. & RICHMAN, M. W. 1986 Boundary conditions for plane flows of smooth, nearly elastic, circular disks. *J. Fluid Mech.* **171**, 53–69.

RICHMAN, M. W. 1988 Boundary conditions based upon a modified Maxwellian velocity distribution for flows of identical, smooth, nearly elastic spheres. *Acta Mechanica* **75**, 227–240.

RICHMAN, M. W. & CHOU, C. S. 1988 Boundary effects on granular shear flows of smooth disks. *Z. Angew. Math. Phys.* **39**, 885–901.

RIDGWAY, K. & RUPP, R. 1970 Flow of granular material down chutes. *Chem. Proc. Engng* **51**, 82–85.

SAVAGE, S. B. 1979 Gravity flow of cohesionless granular materials in chutes and channels. *J. Fluid Mech.* **92**, 53–96.

SAVAGE, S. B. & SAYED, M. 1984 Stresses developed by dry cohesionless granular materials in an annular shear cell. *J. Fluid Mech.* **142**, 391–430.

ZHANG, Y. & CAMPBELL, C. S. 1992 The interface between fluid-like and solid-like behavior in two-dimensional granular flows. *J. Fluid Mech.* **237**, 541–568.